Prior expectations induce pre-stimulus sensory templates

Peter Kok[1,2], Pim Mostert[1] and Floris P. de Lange[1]

1. Radboud University Nijmegen, Donders Institute for Brain, Cognition and Behaviour, Kapittelweg 29, 6525 EN Nijmegen, The Netherlands
2. Princeton University, Princeton Neuroscience Institute, 301 Peretsman-Scully Hall, Princeton, NJ 08544

Running title: Expectations induce stimulus templates

Manuscript information: This manuscript contains 145 (Abstract) + 2147 (Introduction + Results + Discussion) words, 3 Figures and 3 figure supplements.

Keywords: prediction; perceptual inference; predictive coding; feature-based expectation; feature-based attention

Author contributions

P.K. and F.d.L. designed the experiment, P.K. and P.M. conducted the experiment, P.K. and P.M. analysed the data, P.K., P.M. and F.d.L. wrote the paper.

Acknowledgements

This work was supported by The Netherlands Organisation for Scientific Research (NWO) to P.K. (Rubicon grant 446-15-004) and F.d.L. (VIDI grant 452-13-016) and the James S McDonnell Foundation to F.d.L. (Understanding Human Cognition 220020373). The authors would like to thank Mariya Manahova for data collection.

Conflict of Interest

The authors declare no competing financial interests.

Contact:
Peter Kok
Princeton Neuroscience Institute
Princeton University
301 Peretsman-Scully Hall, Princeton, NJ 08544
Phone: 1 609 258 8729
E-mail: pkok@princeton.edu

Abstract

Perception can be described as a process of inference, integrating bottom-up sensory inputs and top-down expectations. However, it is unclear how this process is neurally implemented. It has been proposed that expectations lead to pre-stimulus baseline increases in sensory neurons tuned to the expected stimulus, which in turn affects the processing of subsequent stimuli. Recent fMRI studies have revealed stimulus-specific patterns of activation in sensory cortex as a result of expectation, but this method lacks the temporal resolution necessary to distinguish pre- from post-stimulus processes. Here, we combined human MEG with multivariate decoding techniques to probe the representational content of neural signals in a time-resolved manner. We observed a representation of expected stimuli in the neural signal well before they were presented, demonstrating that expectations indeed induce a pre-activation of stimulus templates. These results suggest a mechanism for how predictive perception can be neurally implemented.

Introduction

Perception is heavily influenced by prior knowledge (Helmholtz, 1866; Gregory, 1997; Kersten et al., 2004). Accordingly, many theories cast perception as a process of inference, integrating bottom-up sensory inputs and top-down expectations (Lee and Mumford, 2003; Friston, 2005; Summerfield and de Lange, 2014). However, it is unclear how this integration is neurally implemented. It has been proposed that prior expectations lead to baseline increases in sensory neurons tuned to the expected stimulus (Wyart et al., 2012; SanMiguel et al., 2013; Kok et al., 2014), which in turn leads to improved neural processing of matching stimuli (Kok et al., 2012; Bell et al., 2016). In other words, expectations may induce stimulus templates in sensory cortex, prior to the actual presentation of the stimulus. Alternatively, top-down influences in sensory cortex may exert their influence only after the bottom-up stimulus has been initially processed, and the integration of the two sources of information may become apparent only during later stages of sensory processing (Rao et al., 2012).

The evidence necessary to distinguish between these hypotheses has been lacking. fMRI studies have revealed stimulus-specific patterns of activation in sensory cortex as a result of expectation (Kok et al., 2014; Hindy et al., 2016), but this method lacks the temporal resolution necessary to distinguish pre- from post-stimulus periods. Here, we combined MEG with multivariate decoding techniques to probe the representational content of neural signals in a time-resolved manner (Cichy et al., 2014; King and Dehaene, 2014; Mostert et al., 2015; Myers et al., 2015). We trained a forward model to decode the orientation of task-irrelevant gratings from the MEG signal (Brouwer and Heeger, 2009, 2011), and applied this decoder to trials in which participants expected a grating of a particular orientation to be presented. This analysis revealed a neural representation of the expected grating that resembled the neural signal evoked by an actually presented grating. This representation was present already before stimulus presentation, demonstrating that expectations can indeed induce the pre-activation of stimulus templates.

Results

Participants were exposed to auditory cues that predicted the likely orientation (45° or 135°) of an upcoming grating stimulus (Figure 1A-B). This grating was followed by a second grating that differed slightly from the first in terms of orientation and contrast. In separate runs of the MEG session, participants performed either an orientation or contrast discrimination task on the two gratings (see Materials and Methods for details).

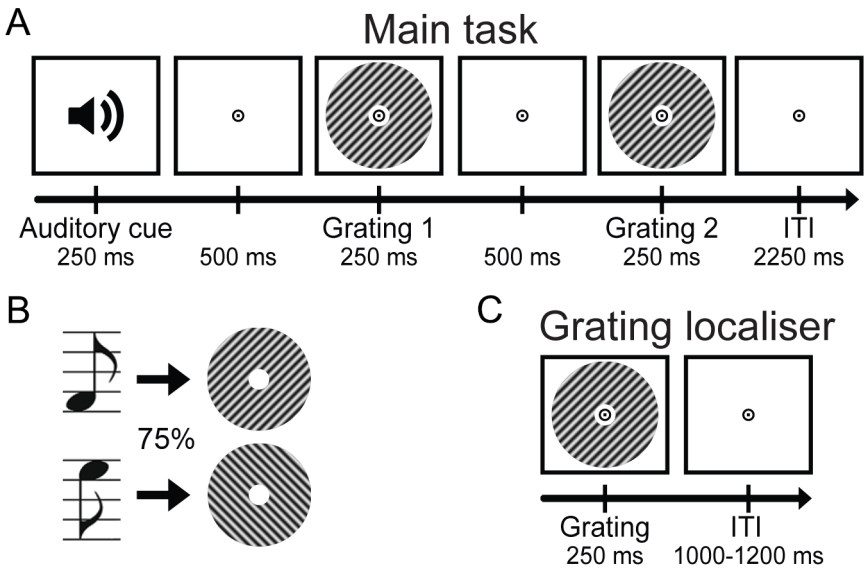

Figure 1. Experimental paradigm. (**A**) Each trial started with an auditory cue that predicted the orientation of the subsequent grating stimulus. This first grating was followed by a second one, which differed slightly from the first in terms of orientation and contrast. In separate runs, participants performed either an orientation or contrast discrimination task on the two gratings. (**B**) Throughout the experiment, two different tones were used as cues, each one predicting one of the two possible orientations (45° or 135°) with 75% validity. These contingencies were flipped halfway through the experiment. (**C**) In separate grating localiser runs, participants were exposed to task-irrelevant gratings while they performed a fixation dot dimming task.

Behavioural results. Participants were able to discriminate small differences in orientation (3.9° ± 0.5°, accuracy = 74.0% ± 1.6%, mean ± sem) and contrast (4.6% ± 0.3%, accuracy = 76.6% ± 1.5%) of the cued gratings. There was no significant difference between the two tasks in terms of either accuracy ($F_{1,22}$ = 3.38, p = 0.080) or reaction time (mean RT = 621 ms vs. 603 ms, $F_{1,22}$ = 1.46, p = 0.24). Overall, accuracy and reaction times were not influenced by whether the cued grating had the expected or the unexpected orientation (accuracy: $F_{1,22}$ = 0.21, p = 0.65; RT: $F_{1,22}$ = 0.03, p = 0.87), nor was there an interaction between task and expectation (accuracy: $F_{1,22}$ = 0.96, p = 0.34; RT: $F_{1,22}$ = 0.42, p = 0.52). Note that these discrimination tasks were orthogonal to the expectation manipulation, in the sense that the expectation cue provided no information about the likely correct choice.

During the grating localiser (Figure 1C, see Materials and Methods for details), participants correctly detected 91.2% ± 1.6% (mean ± sem) of fixation flickers, and incorrectly pressed the button on 0.2% ± 0.1% of trials, suggesting that participants were successfully engaged by the fixation task.

MEG results – Localiser orientation decoding. As mentioned, participants were exposed to auditory cues that predicted the likely orientation of an upcoming grating stimulus. The question we wanted to answer was whether the expectations induced by these auditory cues would evoke templates of the visual stimuli prior to the presentation of the gratings. To be able to uncover such sensory templates, we trained a decoding model to reconstruct the orientation of (task-irrelevant) visual gratings (Figure 1C) from the MEG signal, in a time-resolved manner. First, we found that this model was highly accurate at reconstructing the orientation of such gratings from the MEG signal (Figure 2). Grating orientation could be decoded across an extended period of time (from 40 to 655 ms post-stimulus, p < 0.001, and from 685 to 730 ms, p = 0.018), peaking around 120-160 ms post-stimulus (Figure 2C). Furthermore, in the period around 100 to 330 ms post-stimulus, orientation decoding generalised across time, meaning that a decoder trained on the evoked response at, for example, 120 ms post-stimulus could reconstruct the grating orientation represented in the evoked response around 300 ms, and vice versa (Figure 2D). In other words, certain aspects of the representation of grating orientation were sustained over time.

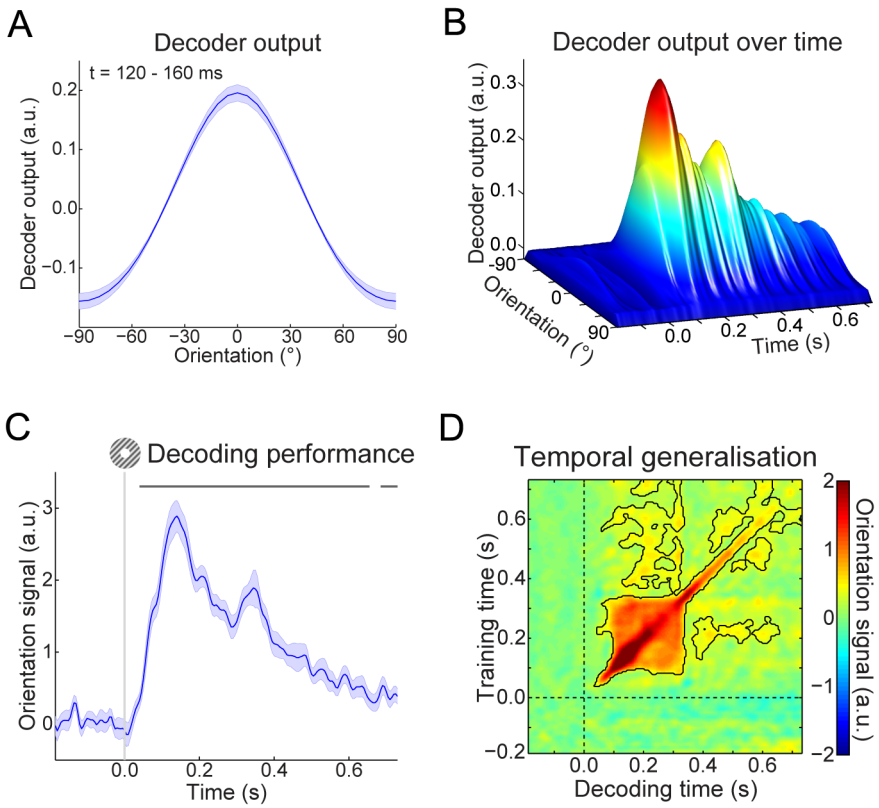

Figure 2. Localiser orientation decoding. (**A**) The output of the decoder consisted of the responses of 32 hypothetical orientation channels, shown here decoders trained and tested on the MEG signal 120-160 ms post-stimulus during the grating localiser (cross-validated). Shaded region represent SEM. (**B**) Decoder output over time, trained and tested in 5 ms steps (sliding window of 29.2 ms), showing the temporal evolution of the orientation signal. (**C**) The response of the 32 orientation channels collapsed into a single metric of decoding performance (see Materials and Methods), over time. Shaded region represent SEM, horizontal lines indicate significant clusters (p < 0.05). (**D**) Temporal generalisation matrix of orientation decoding performance, obtained by training decoders on each time point, and testing all decoders on all time points (as above, steps of 5 ms and a sliding window of 29.2 ms). This method provides insight into the sustained versus dynamical nature of orientation representations (King and Dehaene, 2014). Solid black lines indicate significant clusters (p < 0.05), dashed lines indicate grating onset (t = 0s).

MEG results – Expectation induces stimulus templates. Our main question pertained to the presence of visual grating templates induced by the auditory expectation cues during the main experiment. Therefore, we applied our model trained on task-irrelevant gratings to trials containing gratings that were either validly or invalidly predicted, respectively (Figure 3A). In both conditions, the decoding model trained on task-irrelevant gratings succeeded in accurately reconstructing the orientation of the gratings presented in the main experiment (valid expectation: cluster from training time 60 to 410 ms and decoding time 60 to 400 ms, $p < 0.001$, and from training time 205 to 325 ms and decoding time 400 to 495 ms, $p = 0.045$; invalid expectation: cluster from training time 75 to 225 ms and decoding time 75 to 330 ms, $p = 0.0012$, and from training time 250 to 360 ms and decoding time 195 to 355 ms, $p = 0.027$).

If the cues induced sensory templates of the expected grating, one would expect these to be revealed in the difference in decoding between valid and invalidly predicted gratings (see Material and Methods for details of the subtraction logic). Indeed, this subtraction/analyses demonstrates that the auditory expectation cues induce orientation-specific neural signals (Figure 3A, bottom panel). These signals were present already 40 ms before grating presentation, and extended into the post-stimulus period (from decoding time -40 to 230 ms, $p = 0.0092$, and from 300 to 530 ms, $p = 0.016$). Furthermore, these signals were uncovered when the decoder was trained on around 120 to 160 ms post-stimulus during the grating localiser (Figure 3B), suggesting that these cue-induced signals were similar to those evoked by task-irrelevant gratings. In other words, the auditory expectation cues evoked orientation-specific signals that were similar to sensory signals evoked by the corresponding actual grating stimuli.

In sum, expectations induced pre-stimulus sensory templates that influenced post-stimulus representations as well; invalidly expected gratings had to 'overcome' a pre-stimulus activation of the opposite orientation, while validly expected gratings were facilitated by a compatible pre-stimulus activation (Figure 3 – figure supplement 2A). The post-stimulus carryover of these expectation signals lasted throughout the trial (Figure 3 – figure supplement 2B).

As in previous studies using a similar paradigm (Kok et al., 2012, 2016b), there was no interaction between the effects of the expectation cue and the task (orientation vs. contrast

discrimination) participants performed (no clusters with $p < 0.4$).

In the current study, there was no difference in the overall amplitude of the neural response evoked between validly and invalidly expected gratings (no clusters with $p < 0.4$, Figure 3 – figure supplement 3).

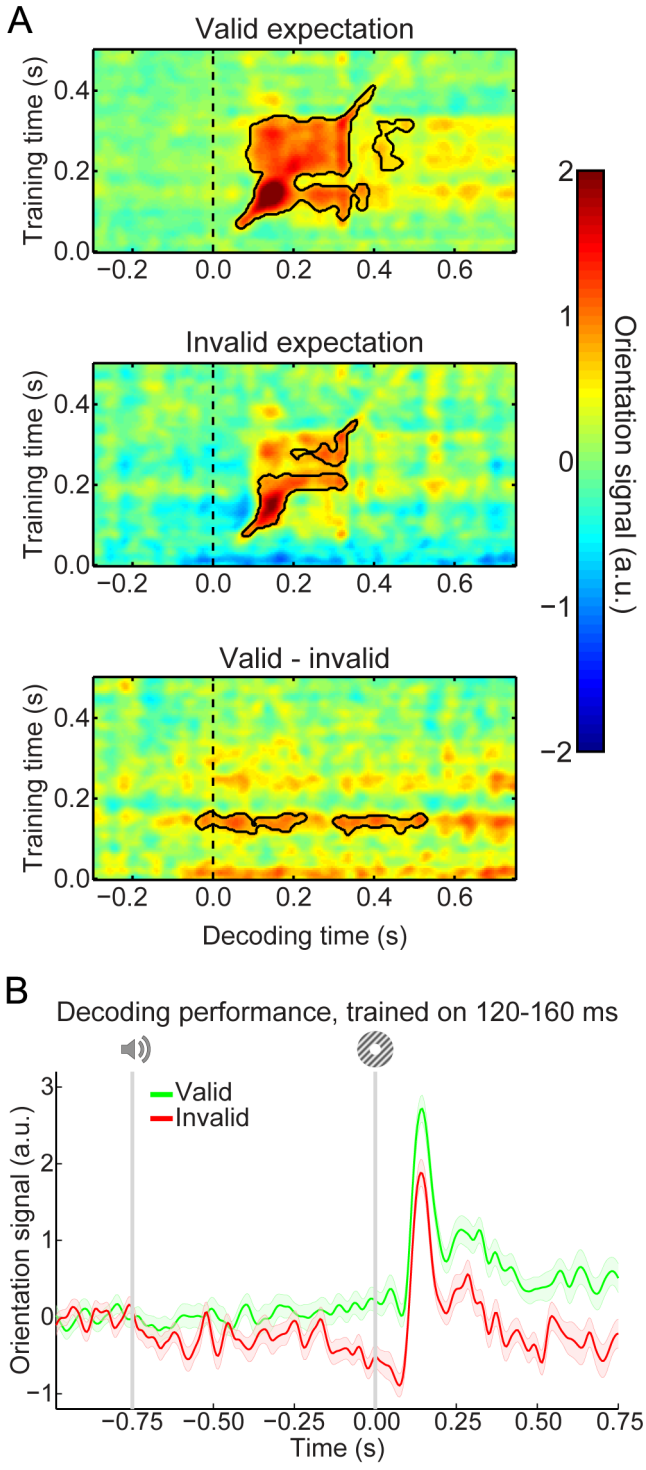

Figure 3. Expectation induces stimulus templates. (**A**) Temporal generalisation matrices of orientation decoding during the main experiment. Decoders were trained on the grating localiser (training time on the y-axis) and tested on the main experiment (time on the x-axis; dashed vertical line indicates t = 0s, onset of the first grating). Decoding shown separately for gratings preceded by a valid expectation (top row), invalid expectation (middle row), and the subtraction of the two conditions (i.e., the expectation cue effect, bottom row). Solid black lines indicate significant clusters ($p < 0.05$). (**B**) Orientation decoding during the main task, averaged over training time 120 – 160 ms post-stimulus during the grating localiser. That is, a horizontal slice through the temporal generalisation matrices above at the training time for which we see a significant cluster of expected orientation decoding, for visualisation. Shaded regions indicate SEM.

The following figure supplements are available for figure 3:

Figure supplement 1. Expectation effects in the absence of low-pass filtering.

Figure supplement 2. Expectation affects orientation decoding throughout the trial.

Figure supplement 3. Event related fields.

Discussion

Here, we show that expectations can induce sensory templates of the expected stimulus already before the stimulus appears. These results extend previous fMRI studies demonstrating stimulus-specific patterns of activation in sensory cortex induced by expectations, which could not resolve whether these templates indeed reflected pre-stimulus expectations, or instead stimulus specific error signals induced by the unexpected omission of a stimulus (Kok et al., 2014; Hindy et al., 2016).

The fact that expectation signals were revealed by a decoder trained on physically presented (but task-irrelevant) gratings suggests that these expectation signals resemble activity patterns induced by actual stimuli. The expectation signal remained present throughout the trial, extending into the post-stimulus period, suggesting the tonic activation of a stimulus template. These results are in line with a recent monkey electrophysiology study (Bell et al., 2016), which showed that neurons in the face patch of IT cortex encode the prior expectation of a face appearing, both prior to and following actual stimulus presentation. When the subsequently presented stimulus is noisy or ambiguous, such a pre-stimulus template could conceivably bias perception towards the expected stimulus (Chalk et al., 2010; Kok et al., 2013; Pajani et al., 2015; John-Saaltink et al., 2016).

What is the source of these cue-induced expectation signals? One candidate region is the hippocampus, which is known to be involved in encoding associations between previously unrelated, discontiguous stimuli (Wallenstein et al., 1998), such as the auditory tones and visual gratings used in the present study. Furthermore, fMRI studies have revealed predictive signals in the hippocampus (Schapiro et al., 2012; Davachi and DuBrow, 2015; Hindy et al., 2016), and Reddy and colleagues (Reddy et al., 2015) reported anticipatory firing to expected stimuli in the medial temporal lobe, including the

hippocampus. One intriguing possibility is that predictive signals from the hippocampus are fed back to sensory cortex (Lavenex and Amaral, 2000; Bosch et al., 2014; Hindy et al., 2016).

In addition to expectation, several other cognitive phenomena have been shown to induce stimulus templates in sensory cortex, such as preparatory attention (Stokes et al., 2009b; Myers et al., 2015), mental imagery (Stokes et al., 2009a; Lee et al., 2012; Albers et al., 2013), and working memory (Harrison and Tong, 2009; Serences et al., 2009). In fact, explicit task preparation can also induce pre-stimulus sensory templates that last into the post-stimulus period (Myers et al., 2015). Note that in the current study the task did not require explicit use of the expectation cues, the task response was in fact orthogonal to the expectation. Furthermore, there was no difference in the expectation signal between runs in which grating orientation was task-relevant (orientation discrimination task) and when it was irrelevant (contrast discrimination task), suggestion expectation may be a relatively automatic phenomenon (den Ouden et al., 2009; Kok et al., 2012). In fact, neural modulations by expectation have even been observed during states of inattention (Näätänen, 1990), sleep (Nakano et al., 2008) and in patients experiencing disorders of consciousness (Bekinschtein et al., 2009). One important question for future research will be to establish whether the same neural mechanism underlies the different cognitive phenomena that are capable of inducing stimulus templates in sensory cortex, or whether different top-down mechanisms are at work. Indeed, it has been suggested that expectation and attention, or task preparation, may have different underlying neural mechanisms (Summerfield and Egner, 2009; Kok et al., 2016b; Summerfield and Egner, 2016). For instance, predictive coding theories suggest that attention may modulate sensory signals in the superficial layers of sensory cortex, while predictions modulate the response in deep layers (Friston, 2005; Kok et al., 2016a).

One may wonder why the current study does not report a modulation of the overall neural response by expectation, while previous studies have found an increased neural response to unexpected stimuli (Summerfield et al., 2008; den Ouden et al., 2009; Alink et al., 2010; Meyer and Olson, 2011; Todorovic et al., 2011; Wacongne et al., 2011), including some using an almost identical paradigm as the current study (Kok et al., 2012, 2016b). Of course, the current study reports a null effect, from which it is hard to draw firm conclusions. However, it is possible that the type of measurement of neural activity

plays a role in the absence of the effect. Most previous studies reporting expectation suppression in visual cortex used fMRI, while the current study used MEG. It is possible that the BOLD signal, a mass-action signal that integrates synaptic and neural activity, as well as integrating over time, is sensitive to certain neural effects that MEG, which is predominantly sensitive to synchronised activity in pyramidal neurons oriented perpendicular to the cortical surface, is not. It is even possible that within MEG, different types of sensors (i.e. magnetometers, planar and axial gradiometers) differ in their sensitivity to expectation suppression (Cashdollar et al., 2016).

Recent theories of sensory processing state that perception reflects the integration of bottom-up inputs and top-down expectations, but ideas diverge on whether the brain continuously generates stimulus templates in sensory cortex to pre-empt expected inputs (Berkes et al., 2011; Pajani et al., 2015; Bell et al., 2016; Fiser et al., 2016), or rather engages in perceptual inference only after receiving sensory inputs (Rao and Ballard, 1999; Bar et al., 2006). Our results are in line with the brain being proactive, constantly forming predictions about future sensory inputs. These findings bring us closer to uncovering the neural mechanisms by which we integrate prior knowledge with sensory inputs to optimise perception.

Materials and Methods

Participants. Twenty-three (15 female, age 26 ± 9, mean ± SD) healthy individuals participated in the experiment. All participants were right-handed and had normal or corrected-to-normal vision. The study was approved by the local ethics committee (CMO Arnhem-Nijmegen, The Netherlands) under the general ethics approval ("Imaging Human Cognition", CMO 2014/288), and the experiment was conducted in accordance with these guidelines. All participants gave written informed consent according to the declaration of Helsinki.

Stimuli. Grayscale luminance-defined sinusoidal grating stimuli (spatial frequency: 1.0 cycles/°) were generated using MATLAB (MathWorks, Natick, MA) in conjunction with the Psychophysics Toolbox (Brainard, 1997). Gratings were displayed in an annulus (outer diameter: 15° of visual angle, inner diameter: 1°), surrounding a black fixation bull's eye (4 cd/m^2), on a gray (580 cd/m^2) background. The visual stimuli were presented with an LCD projector (1024 × 768 resolution, 60 Hz refresh rate) positioned outside the magnetically shielded room, and projected on a translucent screen via two front-silvered mirrors. The projector lag was measured at 36 ms, which was corrected for by shifting the time axis of the data accordingly. The auditory cue consisted of a pure tone (500 or 1000 Hz, 250 ms duration, including 10 ms on and off-ramp time), presented over MEG-compatible earphones.

Experimental design. Each trial consisted of an auditory cue, followed by two consecutive grating stimuli (750 ms SOA between auditory and first visual stimulus) (Figure 1A). The two grating stimuli were presented for 250 ms each, separated by a blank screen (500 ms). A central fixation bull's eye (0.7°) was presented throughout the trial, as well as during the intertrial interval (ITI, 2250 ms). The auditory cue consisted of either a low- (500 Hz) or high-frequency (1000 Hz) tone, which predicted the orientation of the first grating stimulus (45° or 135°) with 75% validity (Figure 1B). In the other 25% of trials, the first grating had the orthogonal orientation. Thus, the first grating had an orientation of either exactly 45° or 135°, and a luminance contrast of 80%. The second grating differed slightly from the first in terms of

282 both orientation and contrast (see below), as well as being in antiphase to the first grating (which had a
283 random spatial phase). The contingencies between the auditory cues and grating orientations were
284 flipped halfway through the experiment (i.e., after four runs), and the order was counterbalanced over
285 subjects.

286 In separate runs (64 trials each, ~4.5 minutes), subjects performed either an orientation or a
287 contrast discrimination task on the two gratings. When performing the orientation task, subjects had to
288 judge whether the second grating was rotated clockwise or anticlockwise with respect to the first
289 grating. In the contrast task, a judgment had to be made on whether the second grating had lower or
290 higher contrast than the first one. These tasks were explicitly designed to avoid a direct relationship
291 between the perceptual expectation and the task response. Subjects indicated their response (response
292 deadline: 750 ms after offset of the second grating) using an MEG-compatible button box. The
293 orientation and contrast differences between the two gratings were determined by an adaptive
294 staircase procedure (Watson and Pelli, 1983), being updated after each trial. This was done to yield
295 comparable task difficulty and performance (~ 75% correct) for the different tasks. Staircase thresholds
296 obtained during one task were used to set the stimulus differences during the other task, in order to
297 make the stimuli as similar as possible in both contexts. As in previous studies using a similar paradigm
298 (Kok et al., 2012, 2016b), there was no interaction between the effects of the expectation cue and the
299 task participants performed, and therefore we collapsed over the two tasks in all MEG analyses.

300 All subjects completed eight runs (four of each task, alternating every two runs, order was
301 counterbalanced over subjects) of the experiment, yielding a total of 512 trials. The staircases were kept
302 running throughout the experiment. Before the first run, as well as in between runs four and five, when
303 the contingencies between cue and stimuli were flipped, subjects performed a short practice run
304 containing 32 trials of both tasks (~4.5 minutes).

305 Interleaved with the main task runs, subjects performed eight runs of a grating localiser task
306 (Figure 1C). Each run (~2 min) consisted of 80 grating presentations (ITI uniformly jittered between 1000
307 and 1200 ms). The grating annuli were identical to those presented during the main task (80% contrast,
308 250 ms duration, 1.0 cycles/°, random spatial phase). Each grating had one of eight orientations

(spanning the 180° space, starting at 0°, in steps of 22.5°), each of which was presented ten times per run in pseudorandom order. A black fixation bull's eye (4 cd/m^2, 0.7° diameter, identical to the one presented during the main task runs) was presented throughout the run. On 10% of trials (counterbalanced across orientations), the black fixation point in the centre of the bull's eye (0.2°, 4 cd/m^2) briefly turned gray (324 cd/m^2) during the first 50 ms of grating presentation. Participants task was to press a button (response deadline: 500 ms) when they perceived this fixation flicker. This simple task was meant to ensure central fixation, while rendering the gratings task-irrelevant. Trials containing fixation flickers were excluded from further analyses.

Finally, participants were exposed to a tone localiser (~1.5 min), presented at the start, end, and halfway through the MEG session. These runs consisted of 81 presentations of the two tones used in the main experiment. Data from these runs were not analysed further.

Prior to the MEG session (1–3 days), all participants completed a behavioural session. The aim of this session was to familiarise participants with the tasks and to initialise the staircase values for both the orientation and the contrast discrimination task (see above). The behavioural session consisted of written instructions and 32 practice trials of each task, followed by four runs (~4.5 min each) of the main experiment (each task twice, alternating between runs, cue contingencies switching between the second and third run). Finally, participants were exposed to one run each of the grating and tone localiser, to familiarise them with the procedure.

MEG recording and preprocessing. Whole-head neural recordings were obtained using a 275-channel MEG system with axial gradiometers (CTF Systems, Coquitlam, BC, Canada) located in a magnetically shielded room. Throughout the experiment, head position was monitored online, and corrected if necessary, using three fiducial coils that were placed on the nasion and on earplugs in both ears (Stolk et al., 2013). If subjects had moved their head more than 5 mm from the starting position they were repositioned during block breaks. Furthermore, both horizontal and vertical electrooculograms (EOGs), as well as an electrocardiogram (ECG) were recorded to facilitate removal of eye- and heart-related

335 artifacts. The ground electrode was placed at the left mastoid. All signals were sampled at a rate of 1200
336 Hz.

337 The data were preprocessed offline using FieldTrip (Oostenveld et al., 2011)
338 (www.fieldtriptoolbox.org). In order to identify artifacts, the variance (collapsed over channels and time)
339 was calculated for each trial. Trials with large variances were subsequently selected for manual
340 inspection and removed if they contained excessive and irregular artifacts. Independent component
341 analysis was subsequently used to remove regular artifacts, such as heartbeats and eye blinks.
342 Specifically, for each subject, the independent components were correlated to both EOGs and the ECG
343 to identify potentially contaminating components, and these were subsequently inspected manually
344 before removal. For the main analyses, data were low-pass filtered using a two-pass Butterworth filter
345 with a filter order of 6 and a frequency cutoff of 40 Hz. To rule out that the temporal smoothing caused
346 by low-pass filtering may have artificially decreased the onset latency of neural signals, we repeated the
347 decoding analyses (see below) on data that were not low-pass filtered (Figure 3 - figure supplement 1).
348 Here, only notch filters were applied at 50, 100 and 150 Hz to remove line noise and its harmonics.
349 Finally, main task data were baseline corrected on the interval of −250 to 0 ms relative to auditory cue
350 onset, and grating localiser data were baseline corrected on the interval of -200 to 0 ms relative to visual
351 grating onset.
352
353 **Event-related field analysis.** Event-related fields (ERFs) were calculated per participant, and subjected
354 to a planar gradient transformation (Bastiaansen and Knösche, 2000) before averaging across
355 participants. The planar transformation simplifies the interpretation of the sensor-level data because it
356 typically places the maximal signal above the source. To avoid differences in the amount of noise when
357 comparing conditions with different numbers of trials, we matched the trial count by randomly selecting
358 a subsample of trials from the conditions with more trials (i.e., valid expectations).
359
360 **Orientation decoding analysis.** To probe sensory representations in the visual cortex, we used a forward
361 modelling approach to reconstruct the orientation of the grating stimuli from the MEG signal (Brouwer

and Heeger, 2009, 2011; Garcia et al., 2013; Myers et al., 2015). The forward modelling approach was two-fold. First, a theoretical forward model was postulated that described the measured activity in the MEG sensors, given the orientation of the presented grating. Second, this forward model was used to obtain an inverse model that specified the transformation from MEG sensor space to orientation space. The forward and inverse models were estimated on the basis of the grating localiser data. The inverse model was then applied to the data from the main experiment, in order to generalise from sensory signals evoked by task-irrelevant gratings to the gratings and expectation signals evoked in the main task. To test the performance of the model we also applied it to the localiser data itself, using a cross-validation approach in which in each iteration one trial of each orientation was used at the test set, and the remaining data were used as the training set.

The forward model was based on work by Brouwer and Heeger (Brouwer and Heeger, 2009, 2011) and involved 32 hypothetical channels, each with an idealised orientation tuning curve. Each channel consisted of a half-wave-rectified sinusoid raised to the fifth power, and the 32 channels were spaced evenly within the 180° orientation space, such that a tuning curve with any possible orientation preference could be expressed exactly as a weighted sum of the channels. Arranging the hypothesised channel activities for each trial along the columns of a matrix **C** (32 channels × *n* trials), the observed data could be described by the following linear model:

$$\mathbf{B} = \mathbf{WC} + \mathbf{N}$$

where **B** are the (*m* sensors × *n* trials) MEG data, **W** is a weight matrix (*m* sensors × 32 channels) that specifies how channel activity is transformed into sensory activity, and **N** are the residuals (i.e., noise).

In order to obtain the inverse model, we estimated an array of spatial filters that, when applied to the data, aimed to reconstruct the underlying channel activities as accurately as possible. In doing so, we extended Brouwer and Heeger's (Brouwer and Heeger, 2009, 2011) approach in three respects. First, since the MEG signal in (nearby) sensors is correlated, we took into account the correlational structure of the noise. Second, we estimated a spatial filter for each orientation channel independently. As a result, the number of channels used in our model was not constrained, whereas the maximum number

of channels would otherwise be dependent on the number of presented orientations. In practice, this resulted in smoothing in orientation space, because the channels were not truly independent. Third, each filter was normalised such that the magnitude of its output matched the magnitude of the underlying channel activity it was designed to recover. Prior to estimating the inverse model, **B** and **C** were demeaned such that their average over trials equalled zero, for each sensor and channel, respectively.

As stated above, the inverse model was estimated on the basis of the grating localiser data. On each localiser trial, one of eight orientations was presented (see above), and the hypothetical responses of each of the channels could thus be calculated for each trial, resulting in the response column vector $\mathbf{c}_{train,i}$, of length n_{train} trials, for each channel *i*. The weights on the sensors $\mathbf{w}_i$ could now be obtained through least squares estimation, for each channel:

$$\mathbf{w}_i = \mathbf{B}_{train}\mathbf{c}_{train,i}^{\mathsf{T}}\left(\mathbf{c}_{train,i}\mathbf{c}_{train,i}^{\mathsf{T}}\right)^{-1}$$

where $\mathbf{B}_{train}$ are the (*m* sensors × n_{train} trials) localiser MEG data. Subsequently, the optimal spatial filter $\mathbf{v}_i$ to recover the activity of the *i*-th channel was obtained as follows (Mostert et al., 2015):

$$\mathbf{v}_i = \frac{\tilde{\Sigma}_i^{-1}\mathbf{w}_i}{\mathbf{w}_i^{\mathsf{T}}\tilde{\Sigma}_i^{-1}\mathbf{w}_i}$$

where $\tilde{\Sigma}_i$ is the regularised covariance matrix for channel *i*. Incorporating the noise covariance in the filter estimation leads to the suppression of noise that arises from correlations between sensors. The noise covariance was estimated as follows:

$$\hat{\Sigma}_i = \frac{1}{n_{train}-1}\boldsymbol{\varepsilon}_i\boldsymbol{\varepsilon}_i^{\mathsf{T}}$$

$$\boldsymbol{\varepsilon}_i = \mathbf{B}_{train} - \mathbf{w}_i\mathbf{c}_{train,i}^{\mathsf{T}}$$

where n_{train} is the number of training trials. For optimal noise suppression, we improved this estimation by means of regularization by shrinkage, using the analytically determined optimal shrinkage parameter (for details, see (Blankertz et al., 2011)), yielding the regularised covariance matrix $\tilde{\Sigma}_i$.

Such a spatial filter was estimated for each hypothetical channel, yielding an *m* sensors × 32 channel filter matrix **V**. Given that we performed our decoding analysis in a time-resolved manner, **V**

was estimated at each time point of the training data, in steps of 5 ms, resulting in array of filter matrices, or decoders. To improve the signal-to-noise ratio, the data were first averaged within a window of 29.2 ms centred on the time point of interest. The window length of 29.2 ms was based on an a priori chosen length of 30 ms, but minus one sample such that the window contained an odd number of samples for symmetric centring (Mostert et al., 2015). These filter matrices could now be applied to estimate the orientation channel responses in independent data – in this case, the trials from the main experiment:

$$\mathbf{C}_{test} = \mathbf{V}^{\mathrm{T}}\mathbf{B}_{test}$$

where $\mathbf{B}_{test}$ are the (m sensors $\times$ n_{test} trials) main experiment data. These channel responses were estimated at each time point of the test data, in steps of 5 ms, with the data being averaged within a window of 29.2 ms at each step. This procedure resulted in a four-dimensional (training time $\times$ testing time $\times$ 32 channel $\times$ n_{test}) matrix of estimated channel responses for each trial in the main experiment. Each trials' channel responses were shifted such that the channel with its hypothetical peak response at the orientation presented on that trial (i.e. 45° or 135°) ended up in the position of the 0° channel, before averaging over trials within each condition (i.e., valid vs. invalid expectation). Thus, the presented orientation was defined as 0°, by convention. Note that for 3D surface plots that show the evolution of channel responses over time (e.g., Figure 2B), the response of the 90° channel (i.e., orthogonal to the presented orientation) was used as a baseline, to avoid negative numbers for visualisation purposes.

To quantify decoding performance, the channel responses for a given condition were converted into polar form and projected onto a vector with angle 0° (the presented orientation, see above).

$$r = |z|\cos\left(\arg\left(z\right)\right), \qquad z = \mathbf{c}^{\mathrm{T}} e^{2i\boldsymbol{\varphi}}$$

where $\mathbf{c}$ is a vector of estimated channel responses, and $\boldsymbol{\varphi}$ is the vector of angles at which the channels peak (multiplied by 2 to project the 180° orientation space onto the full 360° space). The scalar projection r indicates the strength of the decoder signal for the orientation presented on screen. (Note that subtracting the estimated response of the 90° channel from that of the 0° channel yielded virtually

438 identical results, data not shown.) This quantification yielded (training time × testing time) temporal
439 generalisation matrices of orientation decoding performance.

440 In order to isolate any orientation-specific neural signals evoked by the expectation cues, we
441 applied the following subtraction logic. On valid expectation trials, the expected and presented
442 orientations are identical, and thus the orientation signal induced by both the cue and stimulus be
443 expected to be positive, by convention. On invalid expectation trials on the other hand, the expected
444 and presented orientations are orthogonal, and thus the orientation signal induced by the stimulus
445 would be positive and the signal induced by cue would be expected to be negative. Thus, subtracting the
446 orientation decoding signal on invalid trials from that on valid trials would subtract out the stimulus-
447 evoked signal while revealing any cue-induced orientation signal.

448

449 **Statistical testing.** Neural signals evoked by the different conditions were statistically tested using
450 nonparametric cluster-based permutation tests (Maris and Oostenveld, 2007). For ERF analyses, we
451 averaged over the spatial (sensor) dimension, on the basis of independent localisation of the 10 sensors
452 that showed the strongest visual-evoked activity during the grating localiser between 50 and 150 ms
453 post-stimulus. Therefore, our statistical analysis considered one-dimensional (temporal) clusters. For
454 orientation decoding analyses, the data consisted of two-dimensional (training time × testing time)
455 decoding performance matrices, and the statistical analysis thus considered two-dimensional clusters.
456 For both one- and two-dimensional data, univariate *t*-statistics were calculated for the entire matrix and
457 neighbouring elements that passed a threshold value corresponding to a *p*-value of 0.01 (two-tailed)
458 were collected into separate negative and positive clusters. Elements were considered neighbours if
459 they were directly adjacent, either cardinally or diagonally. Cluster-level test statistics consisted of the
460 sum of *t*-values within each cluster, and these were compared to a null distribution of test statistics
461 created by drawing 10,000 random permutations of the observed data. A cluster was considered
462 significant when its *p*-value was below 0.05 (two-tailed).

463 **Figure supplements**

464

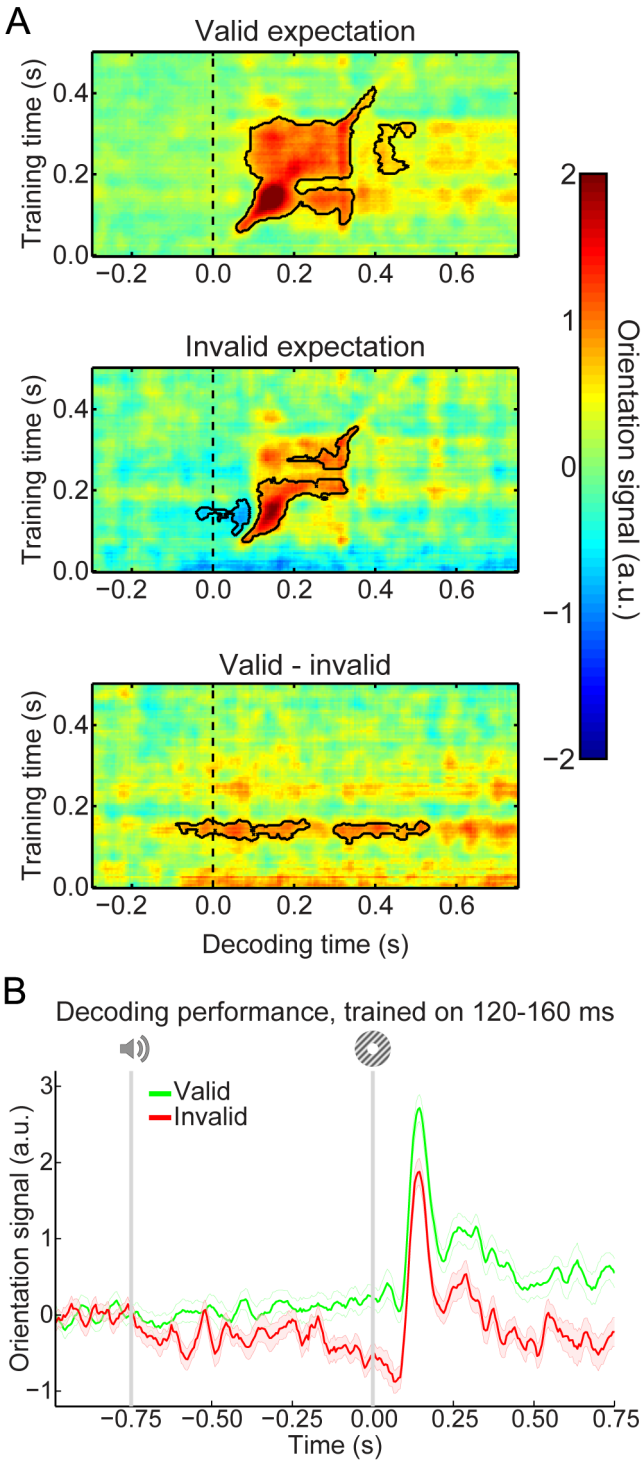

Figure 3 – figure supplement 1. Expectation effects in the absence of low-pass filtering. (**A**) Temporal generalisation matrices of orientation decoding during the main experiment, without low-pass filtering the data. Otherwise, identical to Figure 3A. Solid black lines indicate significant clusters (p < 0.05). (**B**) Orientation decoding during the main task, averaged over training time 120 – 160 ms post-stimulus during the grating localiser. Shaded regions indicate SEM.

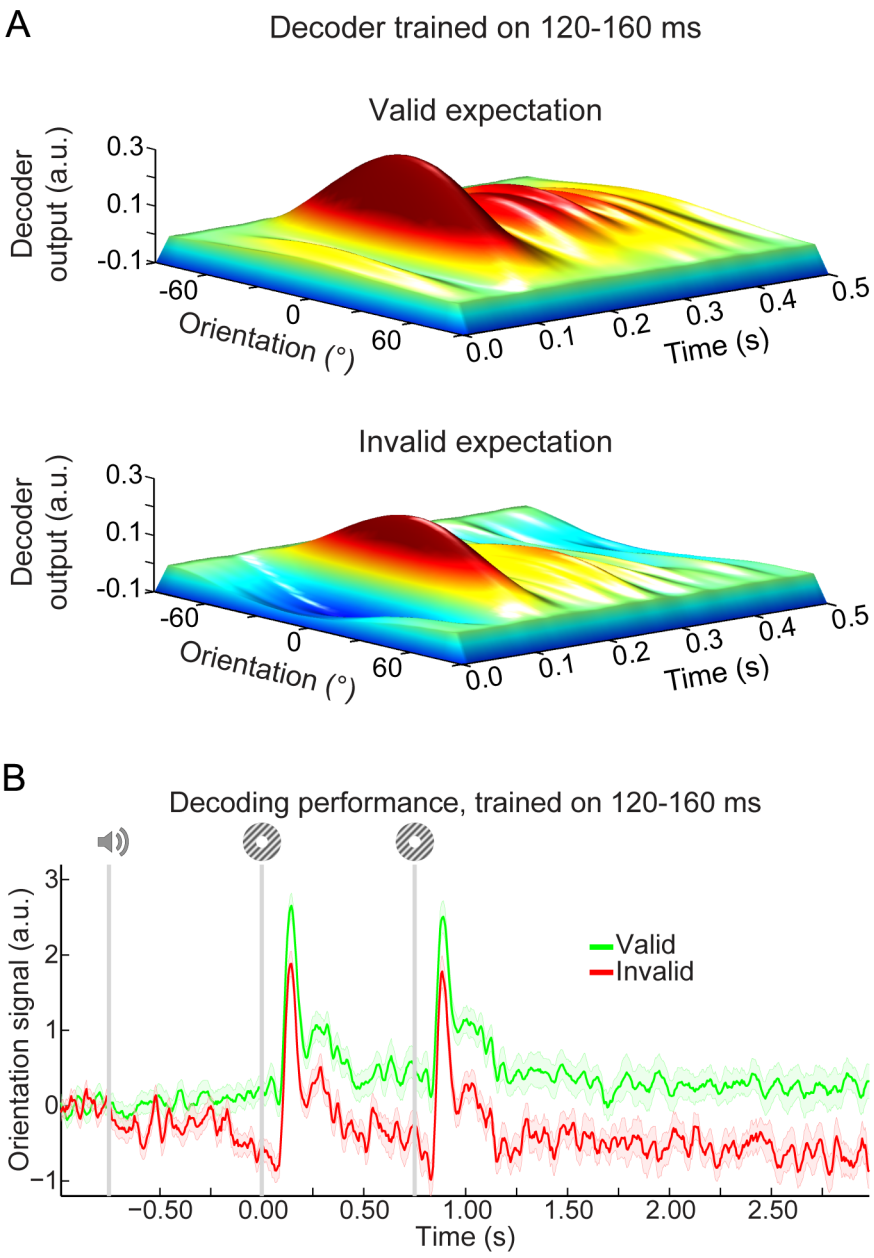

Figure 3 – figure supplement 2. Expectation affects orientation decoding throughout the trial. (**A**) Output of the 32 orientation channels over time, during the main task, separately for gratings preceded by a valid (top panel) and invalid (bottom panel) expectation cue. Here, decoders were trained on 120 – 160 ms post-stimulus during the grating localiser, similar to the data in Figure 3B. That is, this figure depicts similar results as in Figure 3B, but displaying the output of all 32 orientation channels, rather than collapsing the channel responses into a decoding performance score (cf. Figure 2B). (**B**) Orientation decoding during the main task, averaged over training time 120 – 160 ms post-stimulus during the

485 grating localiser. Same as in Figure 3 – figure supplement 1B, but with an extended x-axis, in order to
486 shown the sustained nature of the expectation templates. Shaded regions indicate SEM.
487
488
489
490

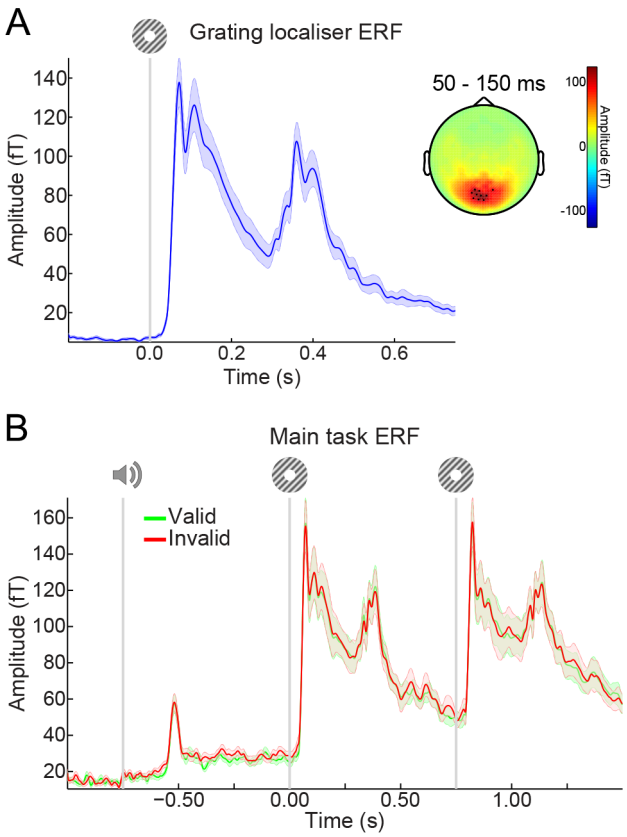

491

492 **Figure 3 – figure supplement 3. Event related fields.** (**A**) Event-related fields during the grating localiser,
493 in the 10 channels showing the largest response from 50 – 150 ms post-stimulus. (**B**) Event-related fields
494 during the main task, in the same 10 channels as in panel A, selected on the basis of the grating localiser
495 response. No significant differences between ERF for validly and invalidly predicted gratings. Shaded
496 regions indicate SEM.

References

Albers AM, Kok P, Toni I, Dijkerman HC, de Lange FP (2013) Shared Representations for Working Memory and Mental Imagery in Early Visual Cortex. Curr Biol 23:1427–1431.

Alink A, Schwiedrzik CM, Kohler A, Singer W, Muckli L (2010) Stimulus Predictability Reduces Responses in Primary Visual Cortex. J Neurosci 30:2960–2966.

Bar M, Kassam KS, Ghuman AS, Boshyan J, Schmid AM, Dale AM, Hämäläinen MS, Marinkovic K, Schacter DL, Rosen BR, others (2006) Top-down facilitation of visual recognition. Proc Natl Acad Sci U S A 103:449–454.

Bastiaansen MCM, Knösche TR (2000) Tangential derivative mapping of axial MEG applied to event-related desynchronization research. Clin Neurophysiol 111:1300–1305.

Bekinschtein TA, Dehaene S, Rohaut B, Tadel F, Cohen L, Naccache L (2009) Neural signature of the conscious processing of auditory regularities. Proc Natl Acad Sci 106:1672–1677.

Bell AH, Summerfield C, Morin EL, Malecek NJ, Ungerleider LG (2016) Encoding of Stimulus Probability in Macaque Inferior Temporal Cortex. Curr Biol 26:2280–2290.

Berkes P, Orban G, Lengyel M, Fiser J (2011) Spontaneous Cortical Activity Reveals Hallmarks of an Optimal Internal Model of the Environment. Science 331:83–87.

Blankertz B, Lemm S, Treder M, Haufe S, Müller K-R (2011) Single-trial analysis and classification of ERP components — A tutorial. NeuroImage 56:814–825.

Bosch SE, Jehee JFM, Fernandez G, Doeller CF (2014) Reinstatement of Associative Memories in Early Visual Cortex Is Signaled by the Hippocampus. J Neurosci 34:7493–7500.

Brainard DH (1997) The Psychophysics Toolbox. Spat Vis 10:433–436.

Brouwer GJ, Heeger DJ (2009) Decoding and Reconstructing Color from Responses in Human Visual Cortex. J Neurosci 29:13992–14003.

Brouwer GJ, Heeger DJ (2011) Cross-orientation suppression in human visual cortex. J Neurophysiol 106:2108–2119.

Cashdollar N, Ruhnau P, Weisz N, Hasson U (2016) The Role of Working Memory in the Probabilistic Inference of Future Sensory Events. Cereb Cortex:bhw138.

Chalk M, Seitz AR, Series P (2010) Rapidly learned stimulus expectations alter perception of motion. J Vis 10:2–2.

Cichy RM, Pantazis D, Oliva A (2014) Resolving human object recognition in space and time. Nat Neurosci 17:455–462.

529 Davachi L, DuBrow S (2015) How the hippocampus preserves order: the role of prediction and context.
530 Trends Cogn Sci 19:92–99.

531 den Ouden HEM, Friston KJ, Daw ND, McIntosh AR, Stephan KE (2009) A Dual Role for Prediction Error in
532 Associative Learning. Cereb Cortex 19:1175–1185.

533 Fiser A, Mahringer D, Oyibo HK, Petersen AV, Leinweber M, Keller GB (2016) Experience-dependent
534 spatial expectations in mouse visual cortex. Nat Neurosci advance online publication Available at:
535 http://www.nature.com/neuro/journal/vaop/ncurrent/full/nn.4385.html [Accessed November
536 28, 2016].

537 Friston K (2005) A theory of cortical responses. Philos Trans R Soc B Biol Sci 360:815–836.

538 Garcia JO, Srinivasan R, Serences JT (2013) Near-Real-Time Feature-Selective Modulations in Human
539 Cortex. Curr Biol 23:515–522.

540 Gregory RL (1997) Knowledge in perception and illusion. Philos Trans R Soc Lond B Biol Sci 352:1121–
541 1127.

542 Harrison SA, Tong F (2009) Decoding reveals the contents of visual working memory in early visual areas.
543 Nature 458:632–635.

544 Helmholtz H von (1866) Treatise on physiological optics, Translated from the third German edition, 1925.
545 Menasha, WI: The Optical Society of America.

546 Hindy NC, Ng FY, Turk-Browne NB (2016) Linking pattern completion in the hippocampus to predictive
547 coding in visual cortex. Nat Neurosci 19:665–667.

548 John-Saaltink ES, Kok P, Lau HC, Lange FP de (2016) Serial Dependence in Perceptual Decisions Is
549 Reflected in Activity Patterns in Primary Visual Cortex. J Neurosci 36:6186–6192.

550 Kersten D, Mamassian P, Yuille A (2004) Object Perception as Bayesian Inference. Annu Rev Psychol
551 55:271–304.

552 King J-R, Dehaene S (2014) Characterizing the dynamics of mental representations: the temporal
553 generalization method. Trends Cogn Sci 18:203–210.

554 Kok P, Bains LJ, van Mourik T, Norris DG, de Lange FP (2016a) Selective Activation of the Deep Layers of
555 the Human Primary Visual Cortex by Top-Down Feedback. Curr Biol 26:371–376.

556 Kok P, Brouwer GJ, van Gerven MAJ, de Lange FP (2013) Prior Expectations Bias Sensory Representations
557 in Visual Cortex. J Neurosci 33:16275–16284.

558 Kok P, Failing MF, de Lange FP (2014) Prior Expectations Evoke Stimulus Templates in the Primary Visual
559 Cortex. J Cogn Neurosci 26:1546–1554.

560 Kok P, Jehee JFM, de Lange FP (2012) Less Is More: Expectation Sharpens Representations in the Primary
561 Visual Cortex. Neuron 75:265–270.

562 Kok P, Van Lieshout LLF, De Lange FP (2016b) Local expectation violations result in global activity gain in
563 primary visual cortex. Sci Rep 6:37706.

564 Lavenex P, Amaral DG (2000) Hippocampal-neocortical interaction: a hierarchy of associativity.
565 Hippocampus 10:420–430.

566 Lee S-H, Kravitz DJ, Baker CI (2012) Disentangling visual imagery and perception of real-world objects.
567 NeuroImage 59:4064–4073.

568 Lee TS, Mumford D (2003) Hierarchical Bayesian inference in the visual cortex. J Opt Soc Am A 20:1434.

569 Maris E, Oostenveld R (2007) Nonparametric statistical testing of EEG- and MEG-data. J Neurosci
570 Methods 164:177–190.

571 Meyer T, Olson CR (2011) Statistical learning of visual transitions in monkey inferotemporal cortex. Proc
572 Natl Acad Sci 108:19401–19406.

573 Mostert P, Kok P, de Lange FP (2015) Dissociating sensory from decision processes in human perceptual
574 decision making. Sci Rep 5:18253.

575 Myers NE, Rohenkohl G, Wyart V, Woolrich MW, Nobre AC, Stokes MG (2015) Testing sensory evidence
576 against mnemonic templates. eLife 4:e09000.

577 Näätänen R (1990) The role of attention in auditory information processing as revealed by event-related
578 potentials and other brain measures of cognitive function. Behav Brain Sci 13:201–233.

579 Nakano T, Homae F, Watanabe H, Taga G (2008) Anticipatory Cortical Activation Precedes Auditory
580 Events in Sleeping Infants Lauwereyns J, ed. PLoS ONE 3:e3912.

581 Oostenveld R, Fries P, Maris E, Schoffelen J-M (2011) FieldTrip: Open Source Software for Advanced
582 Analysis of MEG, EEG, and Invasive Electrophysiological Data. Comput Intell Neurosci 2011:1:1–
583 1:9.

584 Pajani A, Kok P, Kouider S, de Lange FP (2015) Spontaneous Activity Patterns in Primary Visual Cortex
585 Predispose to Visual Hallucinations. J Neurosci 35:12947–12953.

586 Rao RP, Ballard DH (1999) Predictive coding in the visual cortex: a functional interpretation of some
587 extra-classical receptive-field effects. Nat Neurosci 2:79–87.

588 Rao V, DeAngelis GC, Snyder LH (2012) Neural Correlates of Prior Expectations of Motion in the Lateral
589 Intraparietal and Middle Temporal Areas. J Neurosci 32:10063–10074.

590 Reddy L, Poncet M, Self MW, Peters JC, Douw L, van Dellen E, Claus S, Reijneveld JC, Baayen JC,
591 Roelfsema PR (2015) Learning of anticipatory responses in single neurons of the human medial
592 temporal lobe. Nat Commun 6:8556.

593 SanMiguel I, Widmann A, Bendixen A, Trujillo-Barreto N, Schroger E (2013) Hearing Silences: Human
594 Auditory Processing Relies on Preactivation of Sound-Specific Brain Activity Patterns. J Neurosci
595 33:8633–8639.

596 Schapiro AC, Kustner LV, Turk-Browne NB (2012) Shaping of Object Representations in the Human
597 Medial Temporal Lobe Based on Temporal Regularities. Curr Biol 22:1622–1627.

598 Serences JT, Ester EF, Vogel EK, Awh E (2009) Stimulus-Specific Delay Activity in Human Primary Visual
599 Cortex. Psychol Sci 20:207–214.

600 Stokes M, Thompson R, Cusack R, Duncan J (2009a) Top-Down Activation of Shape-Specific Population
601 Codes in Visual Cortex during Mental Imagery. J Neurosci 29:1565–1572.

602 Stokes M, Thompson R, Nobre AC, Duncan J (2009b) Shape-specific preparatory activity mediates
603 attention to targets in human visual cortex. Proc Natl Acad Sci 106:19569–19574.

604 Stolk A, Todorovic A, Schoffelen J-M, Oostenveld R (2013) Online and offline tools for head movement
605 compensation in MEG. NeuroImage 68:39–48.

606 Summerfield C, de Lange FP (2014) Expectation in perceptual decision making: neural and
607 computational mechanisms. Nat Rev Neurosci 15:745–756.

608 Summerfield C, Egner T (2009) Expectation (and attention) in visual cognition. Trends Cogn Sci 13:403–
609 409.

610 Summerfield C, Egner T (2016) Feature-Based Attention and Feature-Based Expectation. Trends Cogn Sci
611 20:401–404.

612 Summerfield C, Trittschuh EH, Monti JM, Mesulam M-M, Egner T (2008) Neural repetition suppression
613 reflects fulfilled perceptual expectations. Nat Neurosci 11:1004–1006.

614 Todorovic A, van Ede F, Maris E, de Lange FP (2011) Prior Expectation Mediates Neural Adaptation to
615 Repeated Sounds in the Auditory Cortex: An MEG Study. J Neurosci 31:9118–9123.

616 Wacongne C, Labyt E, van Wassenhove V, Bekinschtein T, Naccache L, Dehaene S (2011) Evidence for a
617 hierarchy of predictions and prediction errors in human cortex. Proc Natl Acad Sci 108:20754–
618 20759.

619 Wallenstein GV, Hasselmo ME, Eichenbaum H (1998) The hippocampus as an associator of discontiguous
620 events. Trends Neurosci 21:317–323.

621 Watson AB, Pelli DG (1983) Quest: A Bayesian adaptive psychometric method. Percept Psychophys
622 33:113–120.

623 Wyart V, Nobre AC, Summerfield C (2012) Dissociable prior influences of signal probability and relevance
624 on visual contrast sensitivity. Proc Natl Acad Sci 109:3593–3598.

625